Figure 2 **Structural prediction of *TUBB4A* mutations in the αβ-tubulin heterodimer**

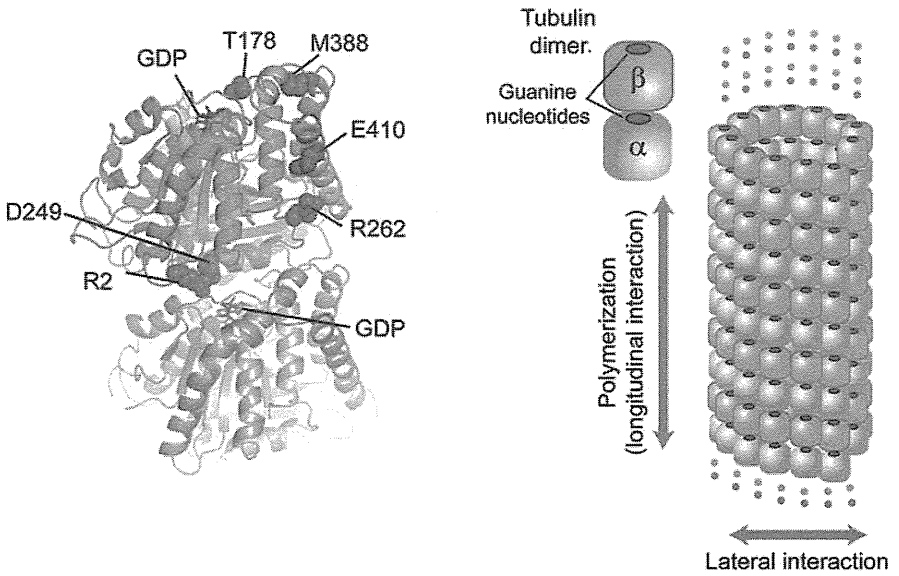

Mapping of disease-causing amino acid mutations on the αβ-tubulin heterodimer (Protein Data Bank code 1JFF) crystal structure, with schematic representation of a tubulin dimer (left) and microtubule segment (right). The α- and β-tubulins are colored gray and green, respectively. Left: The longitudinal interheterodimer interface of β-tubulin (which interacts with α-tubulin in a neighboring αβ heterodimer) is colored pink,[24] and the β-tubulin microtubule-associated protein and motor protein interaction region is colored cyan.[21,22] Side chains of residues altered by the mutations are shown in space-filling representation in red. Helices, β-sheets, and loops are shown as ribbons, arrows, and threads, respectively, and nucleotides are blue sticks. Right: Tubulin heterodimers polymerize longitudinally to form protofilaments (longitudinal interaction), then laterally interact with each other to form microtubules (lateral interaction). Blue circles represent guanine nucleotide-binding pockets of α- and β-tubulins.

mutations are reported to cause the spectrum of neurologic disorders resulting from neural migration, differentiation, and axon guidance and maintenance abnormalities,[25] demonstrating the importance of αβ-tubulin heterodimers in the nervous system.

In this study, we identified 6 missense *TUBB4A* mutations, 5 of which are novel, in 6 of 7 patients with H-ABC and 2 of 7 patients initially diagnosed with unclassified hypomyelinating leukoencephalopathy. Of the patients with H-ABC, all 6 patients with *TUBB4A* mutations showed typical H-ABC, supporting that H-ABC is a distinct disease entity caused by *TUBB4A* abnormality. We did not detect any *TUBB4A* mutations in one patient with atypical H-ABC. This may be because this patient has a clinically similar, but different disease, possibly caused by a different mutated gene.

We report a *TUBB4A* mutation in 2 patients with preserved basal ganglia. Their brain MRI findings are similar to patients with *POLR3A* or *POLR3B* mutations, rather than H-ABC. However, it is notable that both patients showed apparent extrapyramidal signs, to suggest functional impairment. Accompanying extrapyramidal features are extremely atypical in patients with either *POLR3A* or *POLR3B* mutations.[9,11] Furthermore, comparing these 2 patients with other typical H-ABC patients with *TUBB4A* mutations, patients with minimal basal ganglia atrophy tend to have a milder clinical course. Both patients have a recurrent missense mutation, c.1228G>A (p.Glu410Lys). Based on our 3-dimensional modeling analysis, the Glu410Lys mutation is predicted to directly impair motor protein and/or MAP interactions with microtubules, while the other mutations identified in patients with typical H-ABC may affect longitudinal interactions for maintaining αβ-tubulin heterodimerization/polymerization. Different effects of the *TUBB4A* mutations on tubulin function may lead to this phenotypic variation. Supporting this hypothesis, the p.Glu410Lys mutation in *TUBB3*, which also directly alters a kinesin motor protein binding site in β-tubulin isotype 3, demonstrates clinically distinct features compared with the other mutations.[30] Therefore, the p.Glu410Lys mutation in *TUBB4A* may contribute to the milder end of the phenotypic spectrum of *TUBB4A* mutations. Additional patients with *TUBB4A* mutations are needed to clinically confirm mutational consequences.

Another important finding is that one of the patients with H-ABC had a p.Arg2Gln mutation, since the p.Arg2Gly mutation has recently been identified in patients from a large DYT4 family.[18,19] DYT4 was described in 1985 in an Australian family that had emigrated from England as whispering dysphonia and generalized dystonia. To date, no other pedigrees

Figure 3 Brain MRI of patients with *TUBB4A* mutations

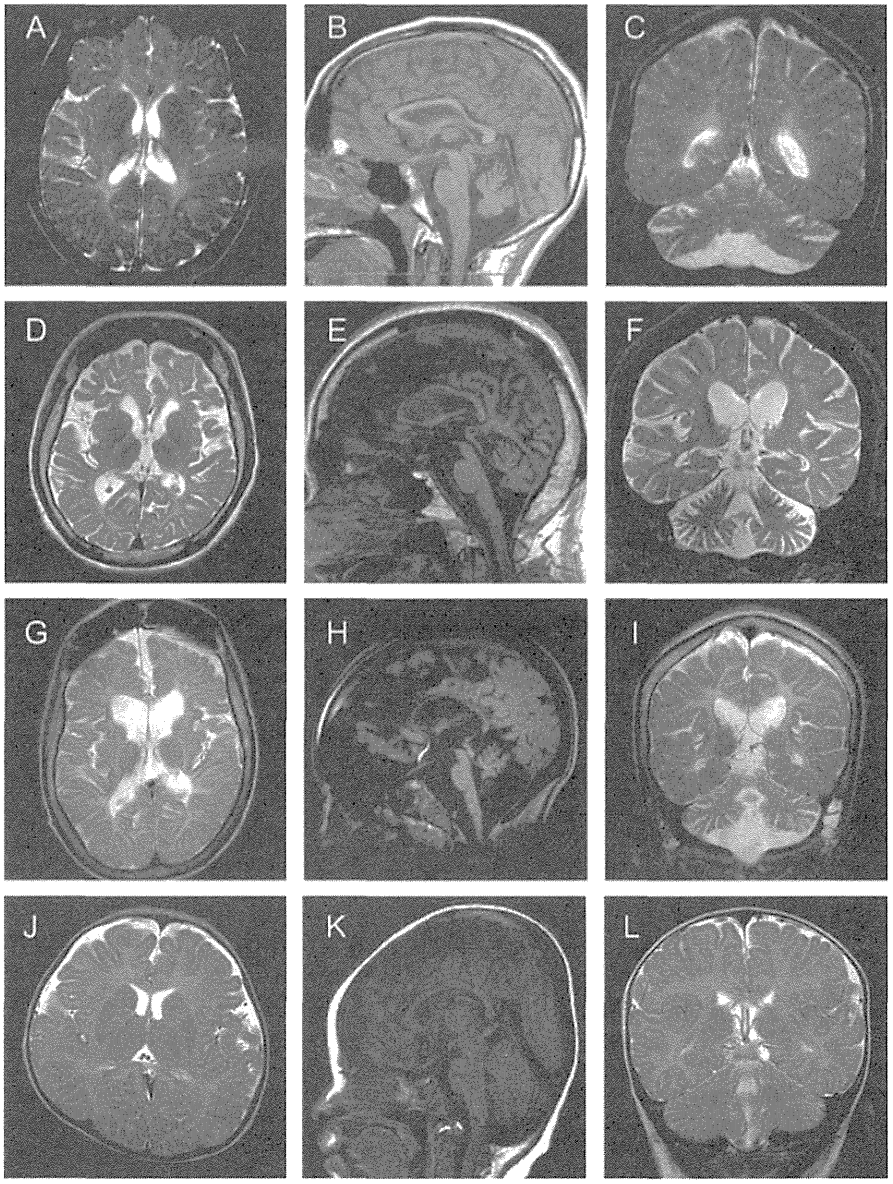

Axial T2-weighted (A, D, G, J), sagittal T1-weighted (B, E, H, K), and coronal T2-weighted (C, F, I, L) images. Patient 1 at 14 years of age (A); patient 1 at 16 years (B, C); patient 2 at 38 years (D–F); patient 3 at 13 years (G–I); and patient 8 at 7 months of age (J–L). All patients show diffuse cerebral white matter hypomyelination with normal (J), mildly reduced (A), or considerably reduced (D, G) white matter volumes. In patient 1, cerebral white matter hypomyelination is unchanged, comparing at 14 (A) and 16 (B, C) years of age. In patient 1, the putamen and the head of the caudate nucleus are normal in size (A). In patient 2, minimal putamen atrophy cannot be excluded (D). The putamen and the head of the caudate nucleus are small or hardly recognizable in patient 3 (G). In patient 8, the putamen is slightly small compared with a healthy control at the same age (J). The globus pallidus and thalamus are normal in size (A, D, G, J). Atrophy of the cerebellar vermis and hemisphere, and corpus callosum was variably observed in 4 patients, but not patient 8 (B, C, E, F, H, I, K, L).

with this phenotype have been reported worldwide.[18] The symptoms typically emerge in the third decade, following a highly penetrant, autosomal dominant mode of inheritance.[31] Brain MRI demonstrates normal structural findings. Arg2 resides within the autoregulatory MREI domain of β-tubulin 4A, which is necessary for autoregulation of the β-tubulin messenger RNA transcript. Site-directed mutagenesis shows that any Arg2 substitution leads to loss of autoregulated instability and increased mutant tubulin subunit levels.[32] Thus, mutations in the MREI domain have been assumed to cause DYT4 rather than H-ABC, because of the different impact on *TUBB4A*.[17] However, our study shows that mutations in the MREI domain can also cause the H-ABC phenotype. The phenotypic difference between the p.Arg2Gly and p.Arg2Gln mutations remains unsolved. Because DYT4 is an extremely rare

syndrome that has only been described in one large pedigree so far, patients of the family may have another modifying factor(s) to spare cerebral white matter abnormalities.

Diffuse hypomyelination syndromes are a heterogeneous group of disorders with overlapping clinical features. Currently, they are categorized based on brain MRI findings, which is very useful in clinical practice. Basal ganglia atrophy specifically distinguishes H-ABC from other hypomyelination disorders. Our study shows that *TUBB4A* mutations associate not only with the typical H-ABC cases but also with some hypomyelinating patients with retained basal ganglia, although notably all patients with *TUBB4A* mutations have extrapyramidal features in common. Our study implies that *TUBB4A* may cause hypomyelinating leukoencephalopathies with either a morphologically or a functionally impaired basal ganglia. Extrapyramidal features may be a key for clinicians to examine *TUBB4A* mutations in genetically unsolved hypomyelinating leukoencephalopathies.

AUTHOR CONTRIBUTIONS

Satoko Miyatake: genetic and clinical data analysis, data interpretation, and drafting/revising of the manuscript. Hitoshi Osaka: clinical data analysis and sample collection. Masaaki Shiina: structural data analysis. Masayuki Sasaki, Jun-ichi Takanashi, Kazuhiro Haginoya, Takahito Wada, Masafumi Morimoto, Naoki Ando, and Yoji Ikuta: clinical data analysis and sample collection. Mitsuko Nakashima, Yoshinori Tsurusaki, and Noriko Miyake: genetic data analysis. Kazuhiro Ogata: structural data analysis. Naomichi Matsumoto: study concept and design, data interpretation, and drafting/revising of the manuscript. Hirotomo Saitsu: study concept and design, genetic data analysis, data interpretation, and drafting/revising of the manuscript.

ACKNOWLEDGMENT

The authors thank all of the participants for their cooperation in this research, and Dr. K. Nishiyama, Ms. K. Takabe, Mr. T. Miyama, Ms. A. Narita, Ms. N. Watanabe, and Ms. S. Sugimoto, from the Department of Human Genetics, Yokohama City University Graduate School of Medicine, for their technical assistance.

STUDY FUNDING

Supported by the Ministry of Health, Labour and Welfare of Japan; the Japan Society for the Promotion of Science (a Grant-in-Aid for Scientific Research [B] [25293085, 25293235]; and a Grant-in-Aid for Scientific Research [A] [13313587]); the Takeda Science Foundation; the fund for Creation of Innovation Centers for Advanced Interdisciplinary Research Areas Program in the Project for Developing Innovation Systems; the Strategic Research Program for Brain Sciences (11105137); and a Grant-in-Aid for Scientific Research on Innovative Areas (Transcription Cycle) from the Ministry of Education, Culture, Sports, Science and Technology of Japan (12024421).

DISCLOSURE

S. Miyatake is funded by research grants from the Yokohama Foundation for Advancement of Medical Science. H. Osaka is funded by research grants from the Ministry of Health, Labour and Welfare of Japan (Research on Rare and Intractable Diseases [H24-Nanchitou-Ippan-072]). M. Shiina and M. Sasaki report no disclosures relevant to the manuscript. J. Takanashi is funded by research grants from the Ministry of Health, Labour and Welfare of Japan (Research on Rare and Intractable Diseases [H24-Nanchitou-Ippan-072]). K. Haginoya, T. Wada, M. Morimoto, N. Ando, Y. Ikuta, M. Nakashima, and Y. Tsurusaki report no disclosures relevant to the manuscript. N. Miyake is funded by research grants from the Ministry of Health, Labour and Welfare of Japan, a Grant-in-Aid for Scientific Research (B) from the Japan Society for the Promotion of Science, and a research grant from the Takeda Science Foundation. K. Ogata is supported by a Grant-in-Aid for Scientific Research on Innovative Areas (Transcription Cycle) from the Ministry of Education, Culture, Sports, Science and Technology of Japan. N. Matsumoto is supported by grants from the Ministry of Health, Labour and Welfare of Japan, a Grant-in-Aid for Scientific Research (A) from the Japan Society for the Promotion of Science, the Takeda Science Foundation, the fund for Creation of Innovation Centers for Advanced Interdisciplinary Research Areas Program in the Project for Developing Innovation Systems, the Strategic Research Program for Brain Sciences, and a Grant-in-Aid for Scientific Research on Innovative Areas (Transcription Cycle) from the Ministry of Education, Culture, Sports, Science and Technology of Japan. H. Saitsu is funded by research grants from a Grant-in-Aid for Scientific Research (B) from the Japan Society for the Promotion of Science, and a research grant from the Takeda Science Foundation. Go to Neurology.org for full disclosures.

Received October 10, 2013. Accepted in final form March 20, 2014.

REFERENCES

1. Schiffmann R, van der Knaap MS. Invited article: an MRI-based approach to the diagnosis of white matter disorders. Neurology 2009;72:750–759.
2. Steenweg ME, Vanderver A, Blaser S, et al. Magnetic resonance imaging pattern recognition in hypomyelinating disorders. Brain 2010;133:2971–2982.
3. Wolf NI, Harting I, Boltshauser E, et al. Leukoencephalopathy with ataxia, hypodontia, and hypomyelination. Neurology 2005;64:1461–1464.
4. Timmons M, Tsokos M, Asab MA, et al. Peripheral and central hypomyelination with hypogonadotropic hypogonadism and hypodontia. Neurology 2006;67:2066–2069.
5. Vazquez-Lopez M, Ruiz-Martin Y, de Castro-Castro P, Garzo-Fernandez C, Martin-del Valle F, Marquez-de la Plata L. Central hypomyelination, hypogonadotrophic hypogonadism and hypodontia: a new leukodystrophy [in Spanish]. Rev Neurol 2008;47:204–208.
6. Bernard G, Thiffault I, Tetreault M, et al. Tremor-ataxia with central hypomyelination (TACH) leukodystrophy maps to chromosome 10q22.3-10q23.31. Neurogenetics 2010;11:457–464.
7. Atrouni S, Daraze A, Tamraz J, Cassia A, Caillaud C, Megarbane A. Leukodystrophy associated with oligodontia in a large inbred family: fortuitous association or new entity? Am J Med Genet A 2003;118A:76–81.
8. Chouery E, Delague V, Jalkh N, et al. A whole-genome scan in a large family with leukodystrophy and oligodontia reveals linkage to 10q22. Neurogenetics 2011;12:73–78.
9. Sasaki M, Takanashi J, Tada H, Sakuma H, Furushima W, Sato N. Diffuse cerebral hypomyelination with cerebellar atrophy and hypoplasia of the corpus callosum. Brain Dev 2009;31:582–587.
10. Bernard G, Chouery E, Putorti ML, et al. Mutations of POLR3A encoding a catalytic subunit of RNA polymerase Pol III cause a recessive hypomyelinating leukodystrophy. Am J Hum Genet 2011;89:415–423.
11. Saitsu H, Osaka H, Sasaki M, et al. Mutations in POLR3A and POLR3B encoding RNA polymerase III subunits cause an autosomal-recessive hypomyelinating leukoencephalopathy. Am J Hum Genet 2011;89:644–651.
12. Tetreault M, Choquet K, Orcesi S, et al. Recessive mutations in POLR3B, encoding the second largest subunit of Pol III, cause a rare hypomyelinating leukodystrophy. Am J Hum Genet 2011;89:652–655.

13. Potic A, Brais B, Choquet K, Schiffmann R, Bernard G. 4H syndrome with late-onset growth hormone deficiency caused by POLR3A mutations. Arch Neurol 2012;69: 920–923.
14. Daoud H, Tetreault M, Gibson W, et al. Mutations in POLR3A and POLR3B are a major cause of hypomyelinating leukodystrophies with or without dental abnormalities and/or hypogonadotropic hypogonadism. J Med Genet 2013;50:194–197.
15. van der Knaap MS, Naidu S, Pouwels PJ, et al. New syndrome characterized by hypomyelination with atrophy of the basal ganglia and cerebellum. AJNR Am J Neuroradiol 2002;23:1466–1474.
16. van der Knaap MS, Linnankivi T, Paetau A, et al. Hypomyelination with atrophy of the basal ganglia and cerebellum: follow-up and pathology. Neurology 2007;69: 166–171.
17. Simons C, Wolf NI, McNeil N, et al. A de novo mutation in the beta-tubulin gene TUBB4A results in the leukoencephalopathy hypomyelination with atrophy of the basal ganglia and cerebellum. Am J Hum Genet 2013;92: 767–773.
18. Hersheson J, Mencacci NE, Davis M, et al. Mutations in the autoregulatory domain of beta-tubulin 4a cause hereditary dystonia. Ann Neurol 2013;73:546–553.
19. Lohmann K, Wilcox RA, Winkler S, et al. Whispering dysphonia (DYT4 dystonia) is caused by a mutation in the TUBB4 gene. Ann Neurol 2013;73:537–545.
20. Lowe J, Li H, Downing KH, Nogales E. Refined structure of alpha beta-tubulin at 3.5 Å resolution. J Mol Biol 2001; 313:1045–1057.
21. Uchimura S, Oguchi Y, Katsuki M, et al. Identification of a strong binding site for kinesin on the microtubule using mutant analysis of tubulin. EMBO J 2006;25:5932–5941.
22. Al-Bassam J, Ozer RS, Safer D, Halpain S, Milligan RA. MAP2 and tau bind longitudinally along the outer ridges of microtubule protofilaments. J Cell Biol 2002;157: 1187–1196.
23. Nawrotek A, Knossow M, Gigant B. The determinants that govern microtubule assembly from the atomic structure of GTP-tubulin. J Mol Biol 2011;412:35–42.
24. Nogales E, Whittaker M, Milligan RA, Downing KH. High-resolution model of the microtubule. Cell 1999; 96:79–88.
25. Tischfield MA, Cederquist GY, Gupta ML Jr, Engle EC. Phenotypic spectrum of the tubulin-related disorders and functional implications of disease-causing mutations. Curr Opin Genet Dev 2011;21:286–294.
26. Wakusawa K, Haginoya K, Kitamura T, et al. Effective treatment with levodopa and carbidopa for hypomyelination with atrophy of the basal ganglia and cerebellum. Tohoku J Exp Med 2006;209:163–167.
27. Hattori A, Ando N, Fujimoto S, Kobayashi S, Ishikawa T, Togari H. A boy with hypomyelination with atrophy of the basal ganglia and cerebellum [in Japanese]. No To Hattatsu 2010;42:42–44.
28. Leandro-Garcia LJ, Leskela S, Landa I, et al. Tumoral and tissue-specific expression of the major human beta-tubulin isotypes. Cytoskeleton 2010;67:214–223.
29. Sullivan KF, Cleveland DW. Sequence of a highly divergent beta tubulin gene reveals regional heterogeneity in the beta tubulin polypeptide. J Cell Biol 1984;99:1754–1760.
30. Chew S, Balasubramanian R, Chan WM, et al. A novel syndrome caused by the E410K amino acid substitution in the neuronal beta-tubulin isotype 3. Brain 2013;136: 522–535.
31. Parker N. Hereditary whispering dysphonia. J Neurol Neurosurg Psychiatry 1985;48:218–224.
32. Yen TJ, Machlin PS, Cleveland DW. Autoregulated instability of beta-tubulin mRNAs by recognition of the nascent amino terminus of beta-tubulin. Nature 1988;334: 580–585.

Am J Physiol Regul Integr Comp Physiol 308: R360–R369, 2015.
First published December 24, 2014; doi:10.1152/ajpregu.00344.2014.

Peripheral oxytocin activates vagal afferent neurons to suppress feeding in normal and leptin-resistant mice: a route for ameliorating hyperphagia and obesity

Yusaku Iwasaki,[1]* Yuko Maejima,[1]* Shigetomo Suyama,[1] Masashi Yoshida,[2] Takeshi Arai,[1] Kenichi Katsurada,[1] Parmila Kumari,[1] Hajime Nakabayashi,[3] Masafumi Kakei,[2] and Toshihiko Yada[1,4]

[1]*Division of Integrative Physiology, Department of Physiology, Jichi Medical University School of Medicine, Tochigi, Japan;* [2]*First Department of Medicine, Saitama Medical Center, Jichi Medical University School of Medicine, Saitama, Japan;* [3]*Health Science Service Center, Kanazawa University, Ishikawa, Japan; and* [4]*Division of Adaptation Development, Department of Developmental Physiology, National Institute for Physiological Sciences, Aichi, Japan*

Submitted 18 August 2014; accepted in final form 15 December 2014

Iwasaki Y, Maejima Y, Suyama S, Yoshida M, Arai T, Katsurada K, Kumari P, Nakabayashi H, Kakei M, Yada T. Peripheral oxytocin activates vagal afferent neurons to suppress feeding in normal and leptin-resistant mice: a route for ameliorating hyperphagia and obesity. *Am J Physiol Regul Integr Comp Physiol* 308: R360–R369, 2015. First published December 24, 2014; doi:10.1152/ajpregu.00344.2014.—Oxytocin (Oxt), a neuropeptide produced in the hypothalamus, is implicated in regulation of feeding. Recent studies have shown that peripheral administration of Oxt suppresses feeding and, when infused subchronically, ameliorates hyperphagic obesity. However, the route through which peripheral Oxt informs the brain is obscure. This study aimed to explore whether vagal afferents mediate the sensing and anorexigenic effect of peripherally injected Oxt in mice. Intraperitoneal Oxt injection suppressed food intake and increased c-Fos expression in nucleus tractus solitarius to which vagal afferents project. The Oxt-induced feeding suppression and c-Fos expression in nucleus tractus solitarius were blunted in mice whose vagal afferent nerves were blocked by subdiaphragmatic vagotomy or capsaicin treatment. Oxt induced membrane depolarization and increases in cytosolic Ca^{2+} concentration ($[Ca^{2+}]_i$) in single vagal afferent neurons. The Oxt-induced $[Ca^{2+}]_i$ increases were markedly suppressed by Oxt receptor antagonist. These Oxt-responsive neurons also responded to cholecystokinin-8 and contained cocaine- and amphetamine-regulated transcript. In obese diabetic *db/db* mice, leptin failed to increase, but Oxt increased $[Ca^{2+}]_i$ in vagal afferent neurons, and single or subchronic infusion of Oxt decreased food intake and body weight gain. These results demonstrate that peripheral Oxt injection suppresses food intake by activating vagal afferent neurons and thereby ameliorates obesity in leptin-resistant *db/db* mice. The peripheral Oxt-regulated vagal afferent neuron provides a novel target for treating hyperphagia and obesity.

nodose ganglion; oxytocin; food intake; obesity; leptin

OXYTOCIN (Oxt) is a neurohypophysial hormone produced in the neurons located in the paraventricular nucleus (PVN) and supraoptic nucleus (SON) of hypothalamus (6). Oxt released from the nerve terminals in the pituitary into peripheral circulation plays an important role in mammalian labor and lactation (24). Oxt is also released within various brain regions from axonal terminals, dendrites, and cell bodies of Oxt neurons, and these central Oxt induce various functions, including social behavior (12), stress responses (37), and promotion of learning and memory (48).

It has been established that Oxt signaling within the central nerves system is implicated in the regulation of food intake. Intracerebroventricular injection of Oxt suppresses food intake, whereas that of Oxt antagonist increases it (2, 3). Meal-related factors, including food intake (22), cholecystokinin (CCK) (36, 43), gastric distension (43), and activation of gastric vagal afferents (50), activate Oxt neurons in the hypothalamus and increase plasma Oxt levels (34, 50, 51). Inversely, fasting reduces Oxt mRNA expression in the hypothalamic PVN (27, 49). Knockdown of Oxt in PVN neurons results in increased food intake and body weight in mice fed normal and high-fat diets (55). The neural pathway downstream of anorexigenic Oxt involves proopiomelanocortin (31) and glucagon-like peptide-1 neurons (44) in the nucleus tractus solitarius (NTS).

Recently, Oxt draws much attention for its therapeutic potential to treat hyperphagia and obesity, as well as autism. Central subchronic infusion of Oxt decreases food intake and body weight in high-fat-diet-induced obese (DIO) mice and rats (10, 55). Interestingly, peripheral subchronic administration of Oxt also reduces food intake and weight gain in DIO mice and rats (10, 30, 33). Thus peripherally administered Oxt mimics the effects of centrally administered Oxt. Here, an important issue is the pathway that conveys the peripheral Oxt's information to the brain for inhibit feeding. The half-life of circulating Oxt is very short, around 1~2 min (15). Furthermore, it has been reported that the transfer of circulating Oxt to the brain is tightly restricted by the blood-brain barrier (BBB), and that only 0.002% of peripherally injected Oxt reaches the central nervous system (32). Previous reports show that intraperitoneal (ip) Oxt administration immediately reduces food intake and induces c-Fos expression in areas of the hindbrain, including NTS and area postrema (AP), that are linked to the control of meal size (30, 33). The NTS and AP are the area where BBB is leaky and Oxt receptors are expressed (54). Therefore, it is plausible that peripheral Oxt could act directly on the neurons in the NTS and AP. On the other hand, NTS is the projection site of vagal afferents (16). The vagal afferent nerves sense the satiety hormones, such as CCK, glucagon-like peptide-1, and peptide YY_{3-36}, and transmit their signals to the brain, thereby decreasing food intake (21). Moreover, vagal afferent neurons express the Oxt receptor mRNA and protein (52). Hence, we hypothesized that peripheral Oxt directly interacts with the vagal afferents, and that this

* Y. Iwasaki and Y. Maejima contributed equally to this work.

Address for reprint requests and other correspondence: Toshihiko Yada, Division of Integrative Physiology, Dept. of Physiology, Jichi Medical University School of Medicine, 3311-1 Yakushiji, Shimotsuke, Tochigi 329-0498, Japan (e-mail: tyada@jichi.ac.jp).

interaction is relayed to signaling to the critical area of the brain and inhibition of feeding behavior.

The present study aimed to clarify whether peripheral Oxt interacts with vagal afferent neurons and, consequently, suppresses food intake. We also explored the therapeutic potential of this interaction for treatment of obesity. We investigated in mice the effects of ip Oxt injection on feeding behavior and c-Fos expression in the NTS, the area innervated by vagal afferents. Furthermore, we examined whether these effects of Oxt on feeding and c-Fos expression were counteracted by subdiaphragmatic vagotomy and systemic capsaicin (CAP) treatment. The effect of Oxt on the membrane potential and cytosolic Ca^{2+} concentration ($[Ca^{2+}]_i$) in vagal afferent neurons isolated from the nodose ganglion (NG) were measured. Finally, we examined whether peripheral Oxt administration could activate vagal afferent pathway and ameliorate hyperphagia and obesity in *db/db* mice with leptin resistance, a condition characteristically associated with human obesity.

RESEARCH DESIGN AND METHODS

Materials. CCK octapeptide (26–33, sulfated form, CCK-8) and Oxt were purchased from Peptide Institute (Osaka, Japan). Oxt receptor antagonist [d(CH_2)$_5$^{1},Tyr(Me)^2,Orn^8]-oxytocin (H4928) was obtained from Bachem, mouse leptin from R&D Systems, and CAP from Sigma.

Animal. Male C57BL/6J mice, aged 8~12 wk, ICR mice aged 6~12 wk (Japan SLC, Shizuoka, Japan), and *db/db* and wild-type BKS mice aged 9~12 wk (CLEA Japan, Tokyo, Japan) were used. The animals were housed in individual cages for at least 1 wk under conditions of controlled temperature (23 ± 1°C), humidity (55 ± 5%), and lighting (light on at 730 and off at 1930). Food and water were available ad libitum. Mice were sufficiently habituated to handling before the experiment of feeding and c-Fos expression. Animal experiments were carried out under approval by the Institutional Animal Experiment Committee of the Jichi Medical University, and in accordance with the Institutional Regulation for Animal Experiments and Fundamental Guideline for Proper Conduct of Animal Experiment and Related Activities in Academic Research Institutions, under the jurisdiction of the Ministry of Education, Culture, Sports, Science and Technology.

CAP treatment and subdiaphragmatic vagotomy. To impair CAP-sensitive sensory nerves, systemic CAP treatment was performed as described (14, 47). In brief, C57BL/6J mice were anesthetized with tribromoethanol (200 mg/kg ip), followed by subcutaneous (sc) administration of CAP at 50 mg/kg body wt (5 ml/kg, solution composition: 10% ethanol, 10% Tween 80, and 80% saline). A second CAP (75 mg/kg sc) injection was performed 2 days later with the same protocol. Finally, CAP (5 mg/kg ip) was injected into the conscious mice 2 days later.

Bilateral subdiaphragmatic vagotomy was performed as described (25). In brief, a midline incision was made to provide wide exposure of the upper abdominal organ in C57BL/6J mice anesthetized with tribromoethanol. The bilateral subdiaphragmatic trunks of vagal nerves along the esophagus were exposed and cut. In the sham operation group, these vagal trunks were exposed but not cut. Vagotomized and sham-operated mice were maintained on a nutritionally complete liquid diet for a human baby (Chilmil, Morinaga, Tokyo, Japan). One to two weeks after the operation, the experiments of feeding or c-Fos expression were performed.

To confirm that CAP treatment and subdiaphragmatic vagotomy were successfully carried out, food intake was measured after ip injection of CCK-8, the substance established to inhibit food intake by activating vagal afferent nerves (46). CCK-8 (4 μg/kg) was ip injected at the light phase (1000) in 16 h-fasted mice, followed by measurement of food intake at 30 min after injection. Anorexigenic effect of CCK-8 was blunted in mice receiving CAP treatment and vagotomy compared with control and sham-operated mice, respectively [means ± SE (number) by unpaired *t*-test]: in the control group, saline 0.50 ± 0.020 g (9) vs. CCK 0.23 ± 0.039 g (8), $P < 0.01$; in CAP-treated group, saline 0.42 ± 0.016 g (6) vs. CCK 0.34 ± 0.035 g (7), not significant; in sham group, saline 1.17 ± 0.13 g (12) vs. CCK 0.28 ± 0.11 g (12), $P < 0.01$; in vagotomized group, saline 1.33 ± 0.20 g (10) vs. CCK 1.02 ± 0.10 g (10), not significant. In contrast, body weight was not different between CAP-treated and control mice and between vagotomized and sham-operated mice (data not shown). These results confirmed that both the CAP treatment and surgical vagotomy successfully blocked the vagal afferent function, while keeping the body's condition sound.

Measurements of food intake after single administration of Oxt. Mice were deprived of food at 1730 with free access to water, ip injected with saline or Oxt dissolved in saline at 1920, and given standard chow (CE-2, CLEA Japan) at 1930 when the dark phase started. Vagotomized and sham-operated C57BL/6J mice were fasted overnight (16 h), ip injected with saline or Oxt at 950, and provided with the liquid diet at 1000.

Conditioned taste aversion test. To accustom mice to a water deprivation schedule, C57BL/6J mice were allowed access to two water bottles for 2 h (1000~1200) for 5 days. On the 6th day, mice were given 0.15% saccharine instead of water for 0.5 h and then injected ip with saline (10 ml/kg), Oxt (200 μg/kg, 10 ml/kg), or lithium chloride (0.15 M, 20 ml/kg). The 7th day was the rest day when mice were given 2 h of normal water access. The 8th day was the test day when two-bottle preference (0.15% saccharine vs. water) test was performed for 0.5 h. Conditioned taste aversion was determined as saccharine preference ratio, saccharine intake/total intake.

Measurements of c-Fos expression in medial NTS. Oxt at 200 μg/kg was ip injected in the vagotomized and sham-operated C57BL/6J mice. At 90 min after injection, these mice were transcardially perfused with 4% paraformaldehyde under anesthesia. The brains were collected, postfixed in the same fixative for overnight at 4°C, and incubated in phosphate buffer containing 30% sucrose for 48 h. Coronal sections (40 μm) of hindbrain were cut using a freezing microtome, collected at 120-μm intervals, and processed for c-Fos immunoreactivity, as described (26). Anti-c-Fos antisera (sc-52, 1:10,000, Santa Cruz Biotechology) were used as the primary antibody. Color was developed with a nickel-diaminobenzidine solution. Neurons immunopositive to c-Fos in medial NTS (bregma −7.32 to −7.76 mm) were counted.

Preparation of single neurons from nodose ganglia. Single neurons were isolated from mouse NGs as described (19). Briefly, NGs were treated 20 min at 37°C with 0.1~0.5 mg/ml collagenase Ia (Sigma), 0.4~0.6 mg/ml dispase II (Roche, Basel, Swiss), 15 μg/ml DNase II type IV (Sigma), and 0.75 mg/ml bovin serum albumin (Sigma) in HEPES-buffered Krebs-Ringer bicarbonate buffer (HKRB) composed of (in mM) 4.7 KCl, 1.2 KH_2PO_4, 129 NaCl, 5 $KaHCO_3$, 1.2 $MgSO_4$, 1.8 $CaCl_2$, and 10 HEPES, with pH adjusted at 7.4 using NaOH supplemented with 5.6 glucose. Single neurons were cultured in Eagle's minimal essential medium containing 5.6 mM glucose supplemented with 10% fetal bovine serum, 100 μg/ml streptomycin, and 100 U/ml penicillin for 12~24 h.

Measurements of $[Ca^{2+}]_i$ in NG neurons. Measurements of $[Ca^{2+}]_i$ in primary cultured NG neurons from ICR, *db/db*, and BKS mice were carried out as described (19). Briefly, following incubation with 2 μM fura 2-AM (DOJINDO, Kumamoto, Japan) for 30 min at 37°C, the cells were mounted in a chamber and superfused with HKRB containing 5.6 mM glucose at 1.3 ml/min at 30°C. Fluorescence ratio images at 510 nm due to excitation at 340 and 380 nm were produced by an Aquacosmos version 2.5 (Hamamatsu Photonics, Shizuoka, Japan). For repeated administration of Oxt, 4-min pulses of Oxt at 10^{-11} M to 10^{-6} M were sequentially applied with washing periods of 8 min or longer.

To exclude possible artifactual data in $[Ca^{2+}]_i$ experiments, the following criteria for responses were used. When $[Ca^{2+}]_i$ changed within 5 min after addition of agents and their amplitudes were at least twice larger than the spontaneous fluctuations of the baseline, they were considered responses. Only the neurons that responded to 55 mM KCl at the end of recordings were analyzed, to secure the soundness of recorded neurons. The amplitude of $[Ca^{2+}]_i$ response to test reagents was normalized to 55 mM KCl in each NG neuron.

Patch-clamp experiments in NG neurons. Perforated whole cell currents recordings in single NG neurons from C57BL/6J mice were performed at room temperature (25°C) using a pipette solution containing (in mM) 40 K_2SO_4, 50 KCl, 5 $MgCl_2$, 0.5 EGTA, 10 HEPES, and amphotericin B (150 μg/ml, Sigma) at pH 7.2 with KOH, as described (20). Electrodes with resistance of 3~5 MΩ were used. Membrane potentials were recorded using an amplifier (Axopatch 200B; Molecular Devices, Foster, CA) in a computer using pCLAMP 9.2 software. Only the neurons that showed stable baseline of membrane potential for more than 3 min were analyzed. When the membrane potential changed with amplitude larger than 1.5 mV and greater than twofold standard deviations of the mean during 2 min before application, it was considered response.

Immunocytochemical identification of cocaine- and amphetamine-regulated transcript neurons. After $[Ca^{2+}]_i$ measurements, the cells were fixed with 4% paraformaldehyde for 2 h at room temperature and processed for immunocytochemistry for cocaine- and amphetamine-regulated transcript (CART), as described (20). Anti-CART (55–102) antibody (H-003–62, 1:10,000, Phoenix Pharmaceuticals) was used. The neurons in which $[Ca^{2+}]_i$ was recorded were correlated with their corresponding immunocytochemical results based on the phase-contrast photographs of the neurons taken right after $[Ca^{2+}]_i$ measurements and the photographs of the neurons after immunostaining (20).

Chronic treatment with Oxt in diabetic db/db mice. Diabetic *db/db* mice aged 11 wk received sc infusion of Oxt at 1,600 $\mu g \cdot kg^{-1} \cdot day^{-1}$ or saline over 2 wk using osmotic minipumps (Alzet, model 2002). Body weight gain and food intake were measured until the 12th day after Oxt infusion.

Statistical analysis. All data were shown as means ± SE. Statistical analysis was performed by one-way ANOVA, followed by Tukey's

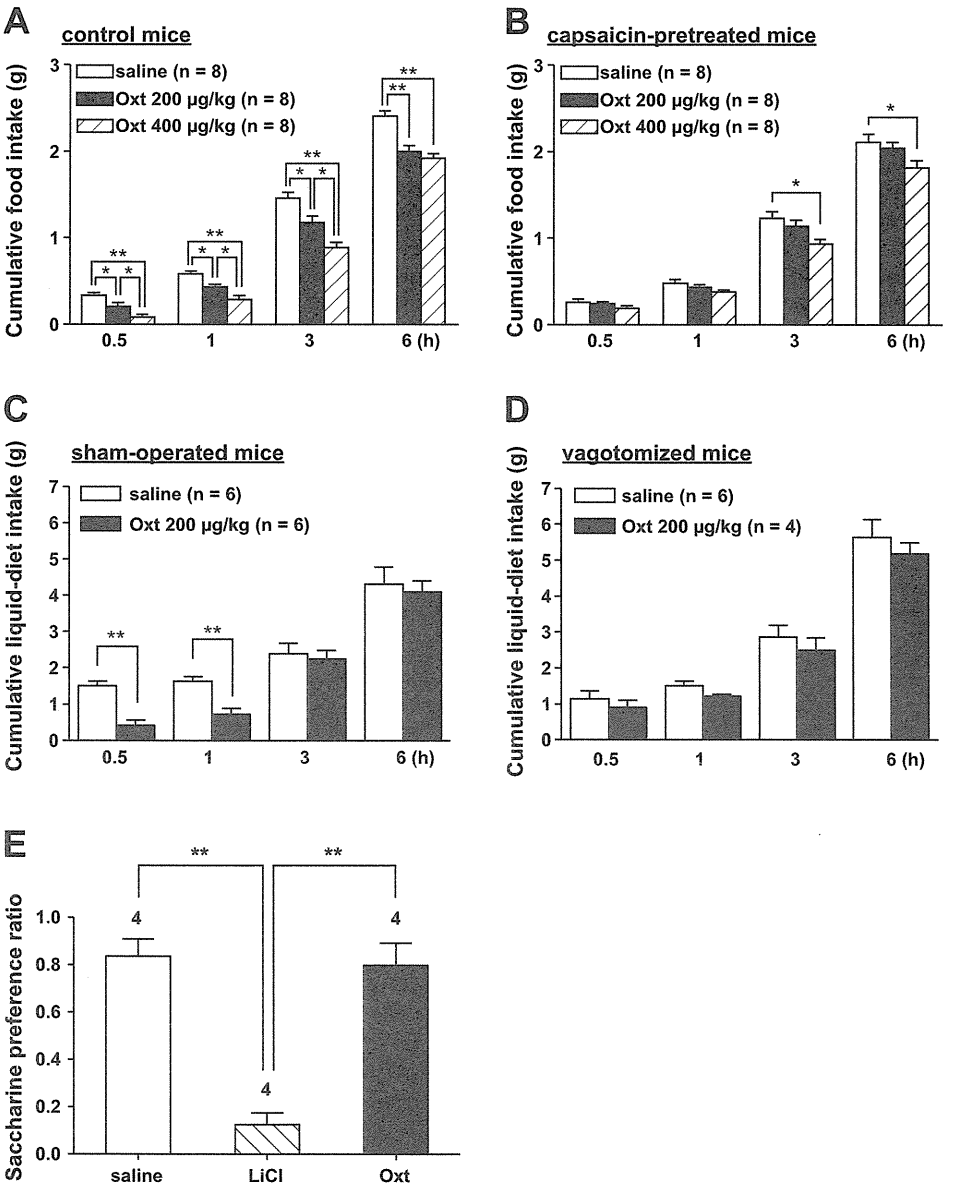

Fig. 1. Intraperitoneal (ip) oxytocin (Oxt) administration suppresses food intake via vagal afferents without aversive behavior. *A* and *B*: ip injection of Oxt at 200 or 400 μg/kg inhibited food intake in C57BL/6J mice, and this effect was abolished or attenuated in the mice whose vagal afferent nerves were blocked by systemic treatment with capsaicin (CAP). Food intake was measured at dark phase just after ip injection of saline (open bar), 200 μg/kg Oxt (solid bar), or 400 μg/kg Oxt (hatched bar) in control (*A*) and CAP-treated mice (*B*). $^*P < 0.05$, $^{**}P < 0.01$ vs. saline by one-way ANOVA followed by Tukey's test. *C* and *D*: inhibition of food intake by 200 μg/kg Oxt was abolished by subdiaphragmatic vagotomy. Liquid-diet intake was measured after ip injection of saline (open bar) or 200 μg/kg Oxt (solid bar) in overnight-fasted mice receiving sham-operation (*C*) and subdiaphragmatic vagotomy (*D*). $^{**}P < 0.01$ vs. saline by unpaired *t*-test. *E*: in the taste aversion test, saccharine preference was measured at 2 days after ip injection of saline, lithium chloride (LiCl; 3 mmol/kg), or Oxt (200 μg/kg). The numbers above each bar indicate the number of experiments. $^{**}P < 0.01$ by one-way ANOVA followed by Tukey's test. Values are means ± SE.

multiple-comparison tests, unpaired or paired t-test, or χ^2 test using the Prism 5 (GraphPad Software). $P < 0.05$ was considered significant.

RESULTS

IP Oxt injection decreases food intake via vagal afferents without aversive behavior. IP injection of Oxt (200 μg/kg and 400 μg/kg) in mice decreased food intake during 0.5–6 h after injection in a dose-dependent manner (Fig. 1*A*), confirming previous report (30). The anorexigenic effect of Oxt at 200 μg/kg was abolished in the mice pretreated with CAP that denervates CAP-sensitive sensory nerves, including vagal afferents (Fig. 1*B*). In contrast, the anorexigenic effect of 400 μg/kg Oxt during 0.5–1 h after injection was markedly impaired, while that during 3–6 h remained partially in CAP-tread mice (Fig. 1*B*). These results suggested that ip Oxt at 200 μg/kg inhibits feeding primarily via sensory nerves, including vagal afferents, while, at a higher dose of 400 μg/kg, it recruits an additional route, which operates during 3–6 h. In the rest of our study, we used 200 μg/kg Oxt that inhibits feeding via vagal afferents.

IP Oxt injection (200 μg/kg) reduced liquid-diet intake at 0.5 and 1 h in the control mice that received sham operation (Fig. 1*C*). In vagotomized mice, in contrast, the anorexigenic effect of Oxt disappeared completely (Fig. 1*D*). Furthermore, ip Oxt injection, unlike lithium chloride, did not influence saccharine preference (Fig. 1*E*), indicating that Oxt did not induce conditioned taste aversion. These results demonstrate that peripheral Oxt administration decreases food intake via interacting with vagal afferents.

IP Oxt induces c-Fos expression in NTS in a vagal afferent-dependent manner. IP injection of 200 μg/kg Oxt into sham-operated mice induced c-Fos expression in medial NTS, to which vagal afferents project (16) (Fig. 2, *A*, *B*, and *E*). In the vagotomized mice, in contrast, ip Oxt injection had no significant effect on the c-Fos expression in medial NTS (Fig. 2, *C*, *D*, and *E*). These results are consistent with the hypothesis that peripheral Oxt activates the neurons

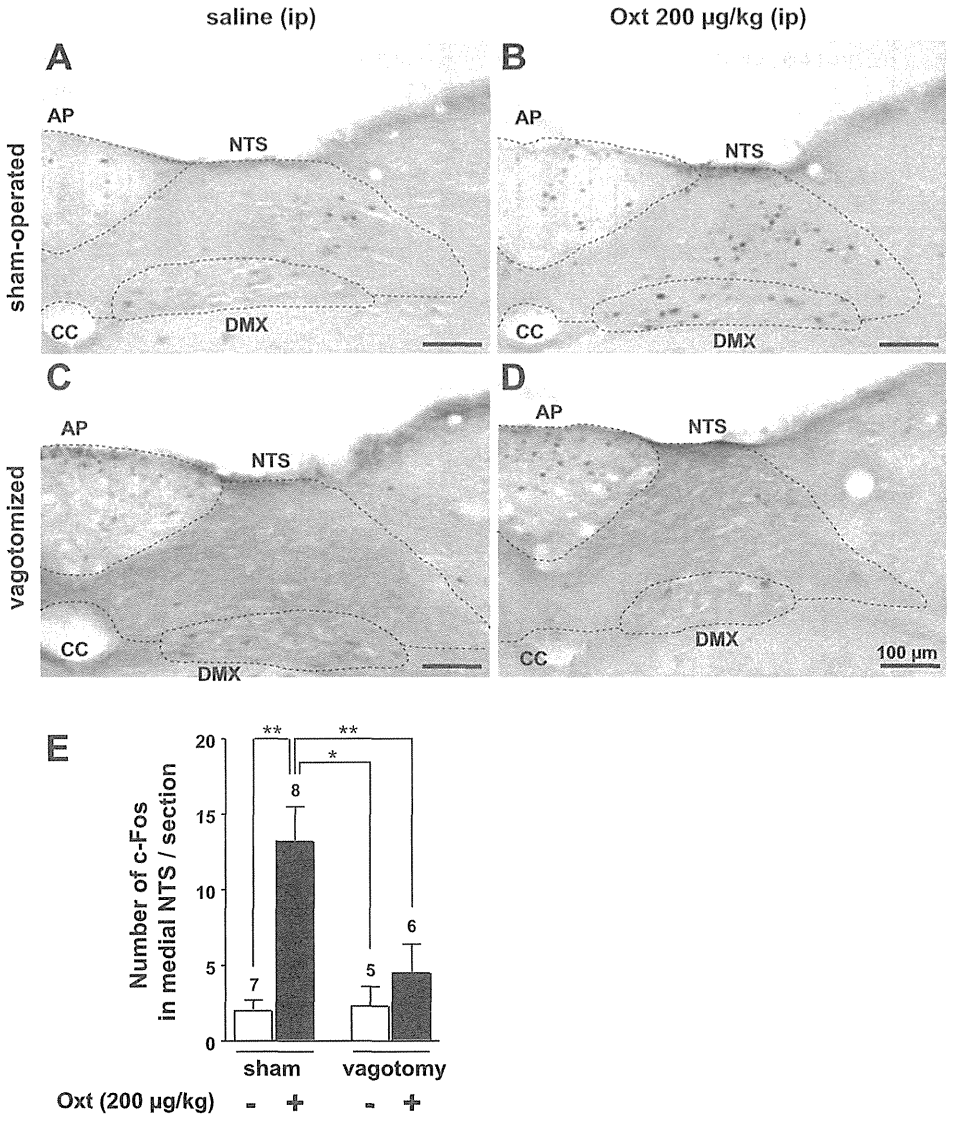

Fig. 2. IP Oxt administration induces c-Fos expression in medial nucleus tractus solitarius (NTS), which is blocked by vagotomy. *A–D*: representative photographs of c-Fos immunoreactivity 90 min after ip administration of saline or 200 μg/kg Oxt in sham-operated (*A*: saline; *C*: Oxt) and vagotomized mice (*B*: saline; *D*: Oxt). IP injection of Oxt (*B*), compared with saline (*A*), induced c-Fos expression in medial NTS in sham-operated mice. *D*: the induction of c-Fos in medial NTS decreased significantly in subdiaphragmatic vagotomized mice. AP, area postrema; CC, central canal; DMX, dorsal motor nucleus. *E*: number of c-Fos immunoreactive neurons in medial NTS after ip saline (open bar) or 200 μg/kg Oxt (solid bar). The number of experiments is indicated above each bar. Values are means ± SE. $*P < 0.05$, $**P < 0.01$ by one-way ANOVA followed by Tukey's test.

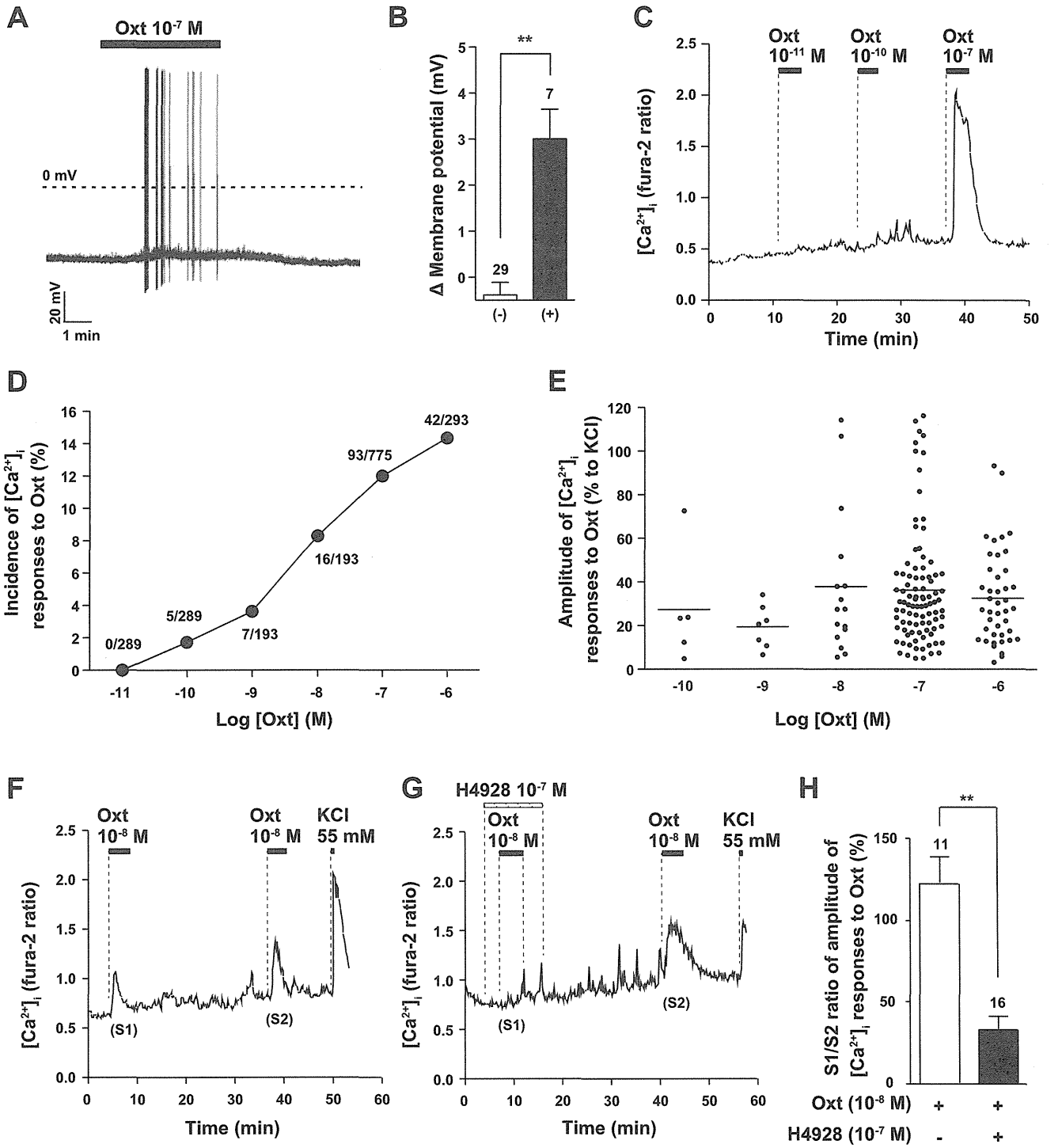

Fig. 3. Oxt induces membrane depolarization, action potential firings, and cytosolic Ca^{2+} concentration ($[Ca^{2+}]_i$) increases via Oxt receptor in single neurons isolated from nodose ganglion (NG). *A*: Oxt at 10^{-7} M induced membrane depolarization and action potential firings in a single NG neuron. Dotted line in *A* indicates 0 mV. Among 36 NG neurons examined, Oxt induced membrane depolarization in 7 neurons and action potential firings in 4 neurons. *B*: the average changes of membrane potential in neurons with (+, $n = 7$) or without (−, $n = 29$) membrane depolarization in response to Oxt. Values are means ± SE. *C*: Oxt at 10^{-10} M and 10^{-7} M but not 10^{-11} M increased $[Ca^{2+}]_i$ in a single NG neuron ($n = 5$). *D* and *E*: concentration-dependent effects of Oxt to increase $[Ca^{2+}]_i$ in single NG neurons, examined by the protocol of repetitive administration shown in *C*. Incidence (*D*) and amplitude (*E*) of $[Ca^{2+}]_i$ responses to Oxt are shown. *D*: numbers around each point indicate the number of neurons that responded to Oxt over that responding to 55 mM KCl. *E*: the amplitude of response to Oxt was normalized to that to 55 mM KCl in each NG neuron, each dot shows value of individual neuron, and the transverse line represents mean. *G*: Oxt (10^{-8} M)-induced $[Ca^{2+}]_i$ increases in single NG neurons were inhibited by Oxt receptor antagonist H4928 (10^{-7} M; $n = 16$). *F*: in control, administration of Oxt twice caused repeated $[Ca^{2+}]_i$ increases ($n = 11$). *H*: the ratio of the peak values of $[Ca^{2+}]_i$ increases in the response to the first Oxt stimulation (S1) over that to the second Oxt stimulation (S2). Values are means ± SE. The numbers above each bar indicate the number of neurons that responded to Oxt. $^{**}P < 0.01$ by unpaired *t*-test.

in medial NTS via a vagal afferent-dependent mechanism.

Oxt induces membrane depolarization, action potential firings, and $[Ca^{2+}]_i$ increases in NG neurons. We measured direct effects of Oxt on membrane potential and $[Ca^{2+}]_i$ in the single neurons isolated from the NG, which is the assembly of cell bodies of all visceral vagal afferent neurons. Administration of Oxt at 10^{-7} M induced the membrane depolarization and action potential firings in a single NG neuron (Fig. 3*A*). Among 36 NG neurons examined, Oxt evoked membrane depolarization (3.00 ± 1.72 mV) in 7 neurons (19.4%) (Fig. 3*B*) and action potential firings (before 0.0639 ± 0.033 Hz vs. during Oxt 0.204 ± 0.102 Hz, $P < 0.05$ by paired *t*-test) in 4 neurons (11.1%). Oxt at 10^{-10} to 10^{-6} M increased $[Ca^{2+}]_i$ in NG neurons, while at 10^{-11} M it had no effect (Fig. 3, *C–E*). Incidence of the $[Ca^{2+}]_i$ response increased as a function of Oxt dose from 10^{-10} to 10^{-7} M and took a plateau value (around 15%) at 10^{-7} and 10^{-6} M (Fig. 3*D*). Thus Oxt increased $[Ca^{2+}]_i$ in NG neurons in a concentration-dependent manner. The $[Ca^{2+}]_i$ response to Oxt was markedly suppressed in the presence of an Oxt receptor antagonist [d$(CH_2)_5^1$, Tyr(Me)^2,Orn^8]-oxytocin (H4928) (Fig. 3, *F–H*), suggesting that Oxt acts on NG neurons via Oxt receptor.

Oxt activates NG neurons that respond to CCK-8 and CAP and that contain CART. It is well known that systemic administration of CCK decreases food intake via directly interacting with vagal afferents (21, 46), and that CAP activates C-type (CAP-sensitive) vagal afferent neurons (13). We examined whether Oxt-responsive NG neurons are distinct from or overlap with CCK-8- or CAP-responsive neurons. Oxt (10^{-7} M), CCK-8 (10^{-8} M), and CAP (10^{-7} M), administered sequentially, evoked $[Ca^{2+}]_i$ increases in 42 (16.4%), 107 (41.8%), and 166 (64.8%) of 256 NG neurons that responded to KCl, respectively (Fig. 4, *A* and *B*). Among 42 NG neurons that responded to Oxt, 41 (95%) responded to CCK-8, and 39 (93%) responded to CAP (Fig. 4, *A* and *B*). In accordance with these $[Ca^{2+}]_i$ results, patch-clamp experiments showed that, among seven NG neurons that responded to Oxt (10^{-7} M) with depolarization, six (85.7%) responded to CCK-8 (10^{-8} M). These results suggest that Oxt primarily targets CCK- and CAP-sensitive NG neurons.

It was reported that the majority of CCK-1 receptor-expressing NG neurons co-express CART (7), suggesting that the CART neuron is involved in CCK-induced inhibition of food intake. We examined whether Oxt interacts with NG neurons containing CART. As shown in Fig. 4, *C* and *D*, 19 of 24 neurons (79.2%) that responded to Oxt with $[Ca^{2+}]_i$ increases were shown to be immunoreactive to CART. The incidence of the CART-immunoreactive neurons was significantly ($P < 0.01$ by χ^2 test) higher in Oxt-responsive neurons (79.2%) than in total neurons (68 of 177 neurons, 38.4%), indicating that Oxt preferentially targets CART neurons.

Oxt activates NG neurons and decreases food intake and body weight in obese diabetic db/db mice. It is considered that peripherally administered leptin decreases food intake partly via interacting with vagal afferents (39, 41), a process possibly involved in homeostatic regulation of body weight. Leptin resistance is often associated with obesity. We investigated the effects of leptin and Oxt on vagal afferent neurons in obese Type 2 diabetic *db/db* mice with mutated leptin receptor and resultant leptin resistance. In NG neurons from wild-type mice, both leptin (10^{-8} M) and Oxt (10^{-7} M) evoked $[Ca^{2+}]_i$ increases (Fig. 5*A*). Leptin increased $[Ca^{2+}]_i$ in 9 out of 285 NG neurons (Fig. 5*C*), and all of these leptin-responsive

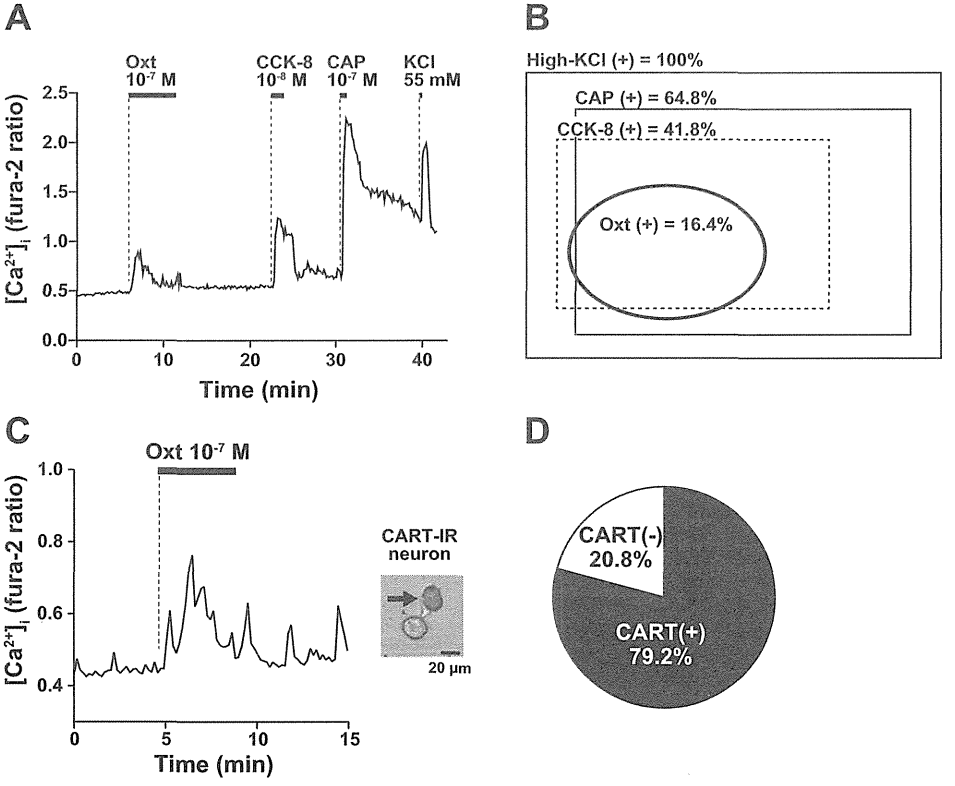

Fig. 4. Oxt-responsive NG neurons substantially overlap cholecystokinin (CCK)-8-responsive NG neurons and contain cocaine- and amphetamine-regulated transcript (CART). *A*: a single NG neuron responded to 10^{-7} M Oxt, 10^{-8} M CCK-8, and 10^{-7} M CAP with increases in $[Ca^{2+}]_i$ ($n = 38$). *B*: overlap of the Oxt-, CCK-8-, and CAP-responsive (+) NG neurons. Among 256 neurons examined, 166 neurons (64.8%) responded to CAP, 107 (41.8%) to CCK, and 42 (16.4%) to Oxt. Among these 42 Oxt-responsive neurons, 38 also responded to both CAP and CCK, while 1 and 3 neurons did not respond to CAP and CCK, respectively. *C*: Oxt at 10^{-7} M increased $[Ca^{2+}]_i$ in a NG neuron that was subsequently proved to be immunoreactive (IR) to CART. *D*: out of 24 NG neurons that responded to Oxt, 19 (79.2%) neurons were IR to CART.